First nuclear genome assembly of an extinct moa species, the little bush moa (*Anomalopteryx didiformis*)

Alison Cloutier[1,2*], Timothy B. Sackton[3], Phil Grayson[1,2], Scott V. Edwards[1,2], Allan J. Baker[4,5¶]

[1]*Department of Organismic and Evolutionary Biology, Harvard University, Cambridge MA USA*

[2]*Museum of Comparative Zoology, Harvard University, Cambridge MA USA*

[3]*Informatics Group, Harvard University, Cambridge MA USA*

[4]*Department of Ecology and Evolutionary Biology, University of Toronto, Toronto ON Canada*

[5]*Department of Natural History, Royal Ontario Museum, Toronto ON Canada*

[¶]*Deceased*

*Corresponding author: alison.cloutier@mail.utoronto.ca

ABSTRACT

High throughput sequencing (HTS) has revolutionized the field of ancient DNA (aDNA) by facilitating recovery of nuclear DNA for greater inference of evolutionary processes in extinct species than is possible from mitochondrial DNA alone. We used HTS to obtain ancient DNA from the little bush moa (*Anomalopteryx didiformis*), one of the iconic species of large, flightless birds that became extinct following human settlement of New Zealand in the 13th century. In addition to a complete mitochondrial genome at 273.5X depth of coverage, we recover almost 900 Mb of the moa nuclear genome by mapping reads to a high quality reference genome for the emu (*Dromaius novaehollandiae*). This first nuclear genome assembly for moa covers approximately 75% of the 1.2 Gbp emu reference with sequence contiguity sufficient to identify 87% of bird universal single-copy orthologs. From this assembly, we isolate 40 polymorphic microsatellites to serve as a community resource for future population-level studies in moa. We also compile data for a suite of candidate genes associated with vertebrate limb development. We find that the wingless moa phenotype is likely not attributable to gene loss or pseudogenization among this candidate set, and identify potential function-altering moa coding sequence variants for future experimental assays.

Key words: little bush moa, ancient DNA, New Zealand, ratite, flightless, microsatellite

INTRODUCTION

The extinct moa of New Zealand (Aves: Dinornithiformes) comprise nine currently recognized species (Bunce et al. 2009) and belong to the Palaeognathae, which encompasses the flightless ratites (ostrich, emu, cassowary, kiwi, rheas, moa, and elephant birds) and the volant,

or flying, tinamous. Extinction of all moa species is thought to have closely followed Polynesian settlement of New Zealand in the late 13th century as the result of direct human exploitation compounded by anthropogenic land-use changes and impacts associated with introduced species (Allentoft et al. 2014; Holdaway et al. 2014).

In addition to a rich history of palaeontological study (reviewed in Worthy and Holdaway 2002), ancient DNA (aDNA) has yielded novel insights into moa biology at almost every turn (Allentoft and Rawlence 2012; Grealy et al. 2017). Cooper et al. (1992) first used aDNA to show that moa are not most closely related to kiwi, indicating independent arrivals of these two lineages to New Zealand. Instead, aDNA places moa as sister to the volant tinamous, consistent with multiple independent losses of flight in ratites (Phillips et al. 2010; Haddrath and Baker 2012; Baker et al. 2014; Cloutier et al. 2018; Sackton et al. 2018). Ancient DNA has also helped clarify moa taxonomy (Baker et al. 2005; Bunce et al. 2009), and was instrumental in identifying extreme reversed sexual size dimorphism that misled some morphological taxonomic designations (Bunce et al. 2003; Huynen et al. 2003). Contributions from ancient DNA have 'clothed' moa by assigning feathers to their species of origin (Rawlence et al. 2009), identified males as the likely incubating sex from eggshell aDNA (Huynen et al. 2010), and investigated moa feeding ecology and parasites using coprolites (Wood et al. 2013a,b).

This diversity of aDNA research testifies to the wealth of relatively well-preserved moa remains (Allentoft and Rawlence 2012). Yet, most studies have relied upon mitochondrial DNA (mtDNA) since mtDNA occurs in high copy number per cell and is therefore more readily recovered than nuclear DNA from subfossil substrates where aDNA is often highly degraded (Allentoft and Rawlence 2012; Hofreiter et al. 2015; Grealy et al. 2017). High throughput sequencing (HTS) has revolutionized the field of aDNA by allowing recovery of these short

segments of nuclear DNA. Unlike mtDNA, which is uniparentally inherited and represents only a tiny fraction of the total genomic 'blueprint' in an individual, nuclear DNA can provide much more detail concerning the evolutionary history and unique adaptations of extinct species (Hofreiter et al. 2015; Grealy et al. 2017). It is therefore likely that we have only just begun to access the available genetic information for moa.

We use high throughput sequencing to recover aDNA from the little bush moa (*Anomalopteryx didiformis*). Little bush moa were distributed in lowland forests across the North and South Islands of New Zealand and were among the smallest of moa species, reaching heights of 50–90 centimeters (Worthy and Holdaway 2002; Bunce et al. 2009). In addition to a complete mitochondrial genome, we report the first nuclear genome for any moa species, assembled by mapping little bush moa reads to a high quality draft genome for the emu (*Dromaius novaehollandiae*, Sackton et al. 2018). We use this moa nuclear genome to isolate polymorphic microsatellites for future population-level studies and also recover coding sequence for a suite of candidate genes to investigate their possible association with flightlessness in moa and other ratites.

MATERIALS AND METHODS

DNA extraction and sequencing

DNA was extracted from a single toe bone of an *Anomalopteryx didiformis* specimen from Pyramid Valley, South Island of New Zealand collected by Trevor Worthy and held in the collections of the Royal Ontario Museum (ROM; Toronto, Canada). The HTS reads reported here were previously used for phylogenetic analysis of palaeognath relationships (Baker et al. 2014), and PCR-based sequences obtained from this specimen have been reported by Haddrath

and Baker (2001), Baker et al. (2005, under sample ID A. did. OH), and Haddrath and Baker (2012, sample TW95).

DNA extraction followed Baker et al. (2005). In brief, the outer 1–2 mm was removed from the bone surface by microblasting with an Airbrasive System (MicroBlaster; Comco, Burbank CA, USA), and 0.2 grams of the remaining material was ground into fine powder. Enzymatic digestion proceeded overnight at 56°C in buffer containing final concentrations of 0.5M EDTA, 200 µg/mL proteinase K, and 0.5% N-laurylsarcosine at pH 8.0 (Hagelberg 1994), and DNA was purified using commercially available silica spin columns (DNeasy Blood & Tissue Kit; Qiagen, Germantown MD, USA). Sample preparation occurred in a dedicated aDNA workspace in the ROM following established best practices (Cooper and Poinar 2000; Knapp et al. 2011).

Library preparation and sequencing was performed by The Centre for Applied Genomics, The Hospital for Sick Children, Toronto, Canada. Library A_didi_CTTGTA was constructed from 200–400 bp size-selected DNA sheared to 200 bp insert size followed by library preparation with the Illumina TruSeq DNA v3 DNA Prep Kit. Paired-end sequencing (2 x 101 bp) was carried out on three lanes of a HiSeq 2500 platform using Illumina v3 chemistry. A second TruSeq library (A_didi_GCCAAT) was prepared from the same input DNA and sequenced on two partial lanes of a HiSeq 2500. Three additional libraries were constructed with the Illumina Nextera XT Sample Preparation Kit. A_didi_CAGAGA and A_didi_CTCTCT used input DNA < 500 bp with no additional shearing, while A_didi_AGGCAG used DNA 500 bp–2 Kb in size subsequently sheared to < 700 bp. These latter barcoded libraries were pooled for sequencing on a single HiSeq 2500 lane.

Read processing and genome assembly

Trimmomatic v. 0.32 (Bolger et al. 2014) was run in paired-end mode for adapter removal and quality trimming and reads with post-trimming length below 25 bp were discarded (options ILLUMINACLIP:[adapter_file]:2:30:10:1:true SLIDINGWINDOW:10:13 MINLEN:25).

A *de novo* mitochondrial genome assembly was built with MITObim v. 1.8 (Hahn et al. 2013) using the published little bush moa mtDNA genome as a starting seed (GenBank accession NC_002779, Haddrath and Baker 2001).

Nuclear sequence assembly first mapped reads to a draft genome for emu (*Dromaius novaehollandiae*; Sackton et al. 2018, BioProject PRJNA433110 [accession pending]), and then re-mapped reads to the initial moa consensus for improved recovery of short and/or variant reads. A random subset of reads was mapped to the emu reference with Stampy v. 1.0.28 (Lunter and Goodson 2011) using default settings to estimate an appropriate substitution parameter. The full data were then mapped to emu with Stampy and this user-specified substitution parameter (estimated at 0.0839). Samtools v. 1.3.1 (Li et al. 2009) was used to filter reads with mapping quality score below 30, and duplicates within each library were marked and removed with Picard Tools v. 2.6.0 (https://broadinstitute.github.io/picard/) before merging mapped reads across libraries. Samtools 'mpileup' was used to output variant call format (VCF) files with minimum mapping quality 30 and base quality 20, and a consensus sequence was called with BCFTools v. 1.2. Reads were re-mapped to this initial consensus with Bowtie2 v. 2.2.9 (Langmead and Salzberg 2012), with subsequent post-processing as above. Assembly completeness was measured with BUSCO v. 2.0 and the aves_odb9 data set (Simão et al. 2015) to search for 4,915 bird universal single-copy orthologs.

Taxonomic read profiling and assessment of DNA damage

Trimmed reads were queried against a custom database containing all avian, bacterial, archaeal, plant (including algae and fungi), and viral sequences from GenBank Release 217 as well as publicly available genomes for the chicken (*Gallus gallus*, galGal4 release, Hillier et al. 2004), North Island brown kiwi (*Apteryx mantelli*, Le Duc et al. 2015), ostrich (*Struthio camelus*, Zhang et al. 2014), white-throated tinamou (*Tinamus guttatus*, Zhang et al. 2014), human (reference genome GRCh38), and the draft emu assembly (Sackton et al. 2018). Reads were mapped in BlastN mode with default parameters in MALT v. 0.3.8 (accessed from http://ab.inf.uni-tuebingen.de/data/software/malt/download/welcome.html), and MEGAN Community Edition v. 6.6.4 (Huson et al. 2016) was used for taxonomic clustering. Patterns of DNA damage were assessed with mapDamage v. 2.0.7 (Jónsson et al. 2013).

Identification of polymorphic microsatellite repeats

MSATCOMMANDER v. 1.0.8 (Faircloth 2008) was used to identify all dinucleotide microsatellites with a minimum of six repeat units and all trinucleotides with at least four repeats in the moa nuclear assembly. Candidate loci with more than 10% uncalled bases (Ns) in the region encompassing the microsatellite and 250 bp of flanking sequence to either side were excluded. Reads mapped to each remaining candidate region were realigned using STR-realigner v. 0.1.01 (Kojima et al. 2016) and genotypes were called with RepeatSeq v. 0.8.2 (Highnam et al. 2013). Heterozygous loci with minimum genotype likelihood ≥ 10 and minimum depth of coverage ≥ 2 for both reference and alternate alleles were retained. Sequence for each retained locus (repeat + flank) was used in blastn searches against draft genomes for seven ratites from Sackton et al. (2018), and the ostrich (Zhang et al. 2014). Blastn hits with evalue $< 1e^{-10}$ were extracted from reference genomes and aligned with MAFFT v. 7.245 (Katoh and Standley 2013).

Tests of selection for candidate limb development genes

Multiple sequence alignments were compiled for a set of candidate genes with established roles in vertebrate limb development (reviewed in Zakany and Duboule 2007; Tanaka 2013; Tickle 2015; Petit et al. 2017; listed in Table 3a) and for genes with potential function-altering variants in the Galapagos cormorant (*Phalacrocorax harrisi*) hypothesized to accompany phenotypic modifications typical of flightless birds (Burga et al. 2017, listed in Table 3b). Gene models were manually curated for ten new draft genome assemblies for palaeognaths (Sackton et al. 2018). Moa coding sequence was obtained from pairwise whole-scaffold alignments of moa to emu using reference emu coordinates (alignments are made available in Dryad Digital Repository [DOI pending]). Sequences from draft palaeognath genomes were combined with available avian sequences from GenBank and cormorant sequences from Burga et al. (2017), and amino acid translations were aligned with MAFFT v. 7.245 (Katoh and Standley 2013). Partial (< 70% of total alignment length) and poorly aligning sequences (< 60% mean pairwise amino acid identity) were removed, and the resulting alignment was used to guide gap insertion in the corresponding nucleotide sequences. GenBank source information, curated gene models, and sequence alignments are made available in Dryad Digital Repository (DOI pending).

We used the adaptive branch-site random effects likelihood model (aBSREL, Smith et al. 2015) in HyPhy v. 2.3.3 (Kosakovsky Pond et al. 2005) to test for lineage-specific selection in moa. We used the RELAX method (Wertheim et al. 2015), also implemented in HyPhy, to test for changes in selection intensity along specified foreground branches. We first tested for changes in moa relative to other ratites by pruning the data set to contain only ratites and then setting moa as the foreground branch and other flightless ratite lineages as the background. Second, we assessed shifts in selection accompanying loss of flight by setting all flightless

lineages as the foreground (including the Galapagos cormorant, penguins, ratites, and inferred flightless ancestors) and all volant lineages as the background. Multiple test correction to control the false discovery rate at 0.05 within each analysis used the qvalue package v. 2.2.0 (Storey 2015) to control for the number of candidate genes analyzed (N= 37) as well as a more conservative approach controlling for the expected genome-wide false discovery rate based on an estimated N= 16,255 homologous orthologous groups of genes (HOGs) in birds identified by Sackton et al. (2018).

Functional effects of moa sequence variants were assessed with PROVEAN v. 1.1.5 (Choi et al. 2012), using a threshold score < -5 to identify possible function-altering variants following Burga et al. (2017). We computed PROVEAN scores for moa substitutions relative to an emu reference sequence and additionally comparing moa to an inferred ancestral sequence for the common moa-tinamou ancestor reconstructed in PAML v. 4.8 under the codon-based model (Yang 2007).

RESULTS AND DISCUSSION

Library characterization and endogenous DNA content

High throughput sequencing yielded 143.4 Gbp of raw data (Table 1, available from NCBI under SRA accession SRP132423). Most data incorporated into the mitochondrial and nuclear genomes described below originated from library A_didi_CTTGTA (Fig. 1A), due in part to greater sequencing effort for this library. Library A_didi_GCCAAT produced fewer reads than expected and had a high level of sequence duplication due to suboptimal cluster density (Table 1). Recovery of moa DNA from the three Nextera libraries was also limited, a result that could reflect a smaller amount of input DNA used in the Nextera protocol and/or a

decreased amount of endogenous DNA in the size fractions assayed for these preparations.

Taxonomic profiling of reads, which represent a mixture of endogenous moa DNA and environmental DNA, assigned taxonomy to 26–35% of reads across libraries (Fig. 1B). The TruSeq libraries contained much higher proportions of reads assigned to Aves (e.g. all birds, 13% and 10% respectively for libraries CTTGTA and GCCAAT, Fig. 1B), with most of these reads further assigned to Palaeognathae (Fig. 1C). Total mapping rates before duplicate removal mirror estimated amounts of endogenous DNA in each library (Table 1, Fig. 1C), suggesting use of a relatively divergent emu reference nevertheless recovered most of the recognizably moa DNA within library extracts. Levels of read duplication (Table 1) further indicate that sequencing saturation was reached to recover the maximum possible amount of endogenous DNA.

Ancient DNA is typically degraded to fragments smaller than 500 bp and displays characteristic post-mortem modifications leading to an excess of purines immediately preceding strand breaks and increasing cytosine (C) to thymine (T) substitutions toward fragment ends (Sawyer et al. 2012; Dabney et al. 2013). We cannot fully assess the extent of DNA damage because library construction for this specimen involved DNA shearing, meaning that fragment ends represent a mixture of naturally occurring DNA breakage as well as strand breaks induced during library preparation. However, mean lengths of mapped reads and estimated insert sizes, especially for the two TruSeq libraries, are consistent with well-preserved DNA (Table 1). Consequently, while we do observe signatures of aDNA damage, the amount of damage appears minimal (Supplemental Fig. S1). These observations are not unprecedented for well-preserved moa specimens. Cooper et al. (2001), Haddrath and Baker (2001), and Baker et al. (2005) successfully amplified moa PCR products 250–600 bp in length, and Cooper et al. (2001)

reported high endogenous DNA content and little DNA damage for samples used to sequence complete mitochondrial genomes. Additionally, both the mitochondrial genome described below and phylogenetic analysis of genome-wide data sets of nuclear markers for this specimen corroborate its aDNA sequence authenticity (Baker et al. 2014; Cloutier et al. 2018; Sackton et al. 2018).

Assembly of mitochondrial and nuclear genomes

We recovered a complete 17,043 bp mitochondrial genome at 273.5X average depth of coverage (DoC) following duplicate removal (Fig. 2A, GenBank accession pending). This new little bush moa assembly spans the entire 1,478 bp control region (D loop), which was not fully represented in the published mtDNA genome assembled from PCR-based sequencing of the same specimen (Haddrath and Baker 2001). The new HTS assembly is near identical to the existing reference, with only 2 SNPs across 775 bp of alignable control region sequence, and five SNPs and three single base pair indels across 15,566 bp lying outside the control region (99.9% identity), and with all differences supported by > 70X DoC in the new HTS assembly. A hypervariable control region 'snippet' diagnostic for moa lineages (McCallum et al. 2013) confirms taxonomic assignment of the sequenced specimen, and a longer (382 bp) segment spanning this region is identical to a haplotype from little bush moa sampled at multiple sites across the South Island of New Zealand (Supplemental Fig. S2, Bunce et al. 2009).

Iterative mapping to a high quality emu reference (Sackton et al. 2018) recovered almost 900 Mbp of the little bush moa nuclear genome (BioProject PRJNA433423, accession pending), or approximately 75% of the 1.2 Gbp emu reference (Fig. 2B, Table 2). Average depth of coverage was 4.3X, with 87% of bases having DoC ≥ 2 (Fig. 2B). Moa sequence was mapped to 1,942 of 2,882 reference emu scaffolds (Fig. 2B, Table 2), with only 0.19% of the total emu

assembly length occurring in scaffolds with no mapped reads. Although moa contigs are relatively short (Table 2, maximum contig length= 12.2 Kb), the average break between contigs is also small (Table 2, mean contig break= 218 bp). Therefore, 87.3% of BUSCO single-copy orthologs for birds were identified in moa, with 75.1% of BUSCOs represented by complete coding sequence (Table 2).

Identification of polymorphic microsatellite markers

Microsatellites offer an appealing option for aDNA studies since these nuclear markers are often highly polymorphic, are spread throughout the genome, and are sufficiently short to allow amplification in degraded samples (Selkoe and Toonen 2006). However, wet-lab approaches for microsatellite isolation are not amenable to degraded aDNA samples, and cross-species amplification of markers from extant taxa are often unsuccessful (Selkoe and Toonen 2006; Allentoft et al. 2009, 2011). High throughput sequencing can circumvent these difficulties by identifying microsatellites directly from sequencing reads in the target species. This approach was employed in moa where Allentoft et al. (2009, 2011) developed six polymorphic microsatellites from GS FLX 454 pyrosequencing reads and demonstrated their utility for studies of moa kinship (Allentoft et al. 2015) and population demography (Allentoft et al. 2014).

Nevertheless, individual HTS reads are often too short to provide appropriate flanking sequence for primer design and candidate loci must still be screened for polymorphism (Allentoft et al. 2011). We therefore use a complementary approach to isolate polymorphic microsatellites from the little bush moa nuclear assembly. We identified 27,114 dinucleotide and 25,171 trinucleotide repeats, approximately half of which met our criteria for inclusion based on flanking sequence contiguity (retaining 14,876 dinucleotides and 13,942 trinucleotides). From these, we identified 40 microsatellites (28 dinucleotides and 12 trinucleotides, Suppl. Table S1)

that are heterozygous in the sequenced individual and hence at least minimally polymorphic in the species as a whole. We offer the realigned BAM files for each locus and alignments to other ratites as a community resource for future studies (Dryad digital repository [DOI pending], an example of each data type is given in Fig. 3). Sequence information across ratites should be especially useful for primer design in conserved regions to avoid null alleles in little bush moa samples, and could also enable amplification of these markers across moa species.

Selection tests in candidate limb development genes

Arguably the most remarkable moa trait is the complete absence of wings. All ratites exhibit some degree of forelimb reduction; however, moa are unique in retaining only a fused scapulocoracoid within the pectoral girdle (Worthy and Holdaway 2002; Huynen et al. 2014). Huynen et al. (2014) recovered moa coding sequence for the T-box transcription factor *TBX5*, which plays a key role in forelimb specification and outgrowth (Tanaka 2013; Tickle 2015; Petit et al. 2017), and demonstrated that moa *TBX5* sequence activates promoters of downstream genes in developing chicken embryos. Therefore, alterations to this coding region alone appear unlikely to underlie the wingless moa phenotype (Huynen et al. 2014). We build upon this work by reporting moa sequence for a more comprehensive suite of candidate genes with established involvement in vertebrate limb development (Table 3a), as well as candidates with putative function-altering variants in the Galapagos cormorant hypothesized to accompany forelimb reduction in this flightless species (Burga et al. 2017, Table 3b).

We recovered moa sequence for all investigated genes, with an average 88% of coding sequence per gene recovered from the moa assembly (Table 3). We found no frameshift mutations and only a single in-frame stop codon in *HOXD4* which, however, occurred at 1X coverage and could represent a sequence artifact (note that this codon was masked by Ns for

further tests). There was no evidence for lineage-specific diversifying selection in moa, with P > 0.05 in aBSREL tests for each gene. RELAX tests also found no significant difference in the strength of selection in moa relative to other ratites for candidate genes with established roles in limb development (Table 3a), but identified a significant intensification of selection in moa *FAT1* and significant relaxation in *GLI2* relative to other ratites among the candidates originating from study of the Galapagos cormorant (Table 3b). However, neither of these results remains significant under a more conservative genome-wide correction for an estimated 16,255 genes in birds rather than correcting only for the set of 37 candidates tested here (both P > 0.05).

RELAX tests also identified seven candidates with significant selective shifts in flightless lineages relative to other birds (Table 3). Of these, we find evidence for intensified selection in three homeobox genes (*HOXA2*, *HOXA4*, and *HOXD4*), and significant relaxation in four genes (*GLI3*, *EVC*, *FAT1*, and *TALPID3*; note that *FAT1* shows intensified selection in moa relative to other ratites, but also relaxed selection in flightless birds generally). However, only the intensification for *HOXA2* remains significant under the more stringent genome-wide false discovery rate correction (P= 0.021).

PROVEAN analysis identified 24 moa sequence variants of possible functional relevance compared to the emu reference (Suppl. Table S2). However, half of these variants (12 of 24) are either shared with other species or are polymorphic in moa, with the emu residue present as an alternative moa allele, indicating that this subset of sites is unlikely to underlie the wingless moa phenotype. Additionally, 16 of the 24 sites display alternative residues in other birds that are often accompanied by PROVEAN scores comparable to moa (Suppl. Table S2). Comparison to an inferred reconstruction of the moa-tinamou common ancestor yielded broadly similar results, with 17 of 19 potentially functionally relevant moa variants identical to those identified from

comparison to the emu reference (Suppl. Table S3).

Putative function-altering variants in the Galapagos cormorant are not shared with other flightless lineages (Suppl. Table S4), indicating that any commonality in the genetic basis for independent losses of flight involving these genes is likely not attributable to convergent or parallel amino acid changes. Burga et al. (2017) also identified a deletion in *CUX1* of the Galapagos cormorant, with experimental assays indicating this gene acts as a transcriptional activator of targets *FAT1* and *OFD1*. As with the other reported Galapagos cormorant variants, the *CUX1* deletion is not shared by moa or other ratites (Suppl. Fig. S3). Altogether, we conclude that loss of wings in moa is not attributable to gene loss or pseudogenization within this candidate gene set, although the functional relevance of variants unique to moa requires further experimental work.

CONCLUSION

This first nuclear genome assembly begins a new chapter in the already extensive history of moa aDNA research. This genomic resource has already proved useful to assemble genome-wide data sets of nuclear markers for phylogenetic inference (Baker et al. 2014; Cloutier et al. 2018; Sackton et al. 2018). Here, we further demonstrate its utility to isolate markers for population-level studies and to investigate sequence evolution in candidate protein coding genes. The relative contributions of coding sequence variation and mutations in noncoding regulatory elements to phenotypic variation constitute an area of active research (Petit et al. 2017; Sackton et al. 2018), and we anticipate that availability of a moa nuclear genome will also contribute to study of regulatory changes associated with flightless phenotypes.

ACKNOWLEDGEMENTS

We thank Trevor Worthy for providing moa source material and Oliver Haddrath for extracting moa aDNA. We thank Sergio Pereira of The Centre for Applied Genomics, The Hospital for Sick Children, Toronto, Canada for overseeing library construction and sequencing. Computations were performed on the GPC supercomputer at the SciNet HPC Consortium funded by Compute Canada, the Government of Ontario, and the University of Toronto, as well as the Odyssey cluster supported by the FAS Division of Science, Research Computing Group at Harvard University. This work was supported by the Natural Science and Engineering Research Council of Canada [to A.J.B.]; the Royal Ontario Museum Governors Fund [to A.J.B.]; and the National Science Foundation [NSF grant DEB 1355343 (EAR 1355292) to A.J.B. and S.V.E.]. This work is dedicated to the memory of coauthor Allan Baker, who was the driving force behind this project but passed away prior to its completion.

LITERATURE CITED

Allentoft ME, Heller R, Holdaway RN, Bunce M. 2015. Ancient DNA microsatellite analyses of the extinct New Zealand giant moa (*Dinornis robustus*) identify relatives within a single fossil site. Heredity 115:481–487.

Allentoft ME, et al. 2014. Extinct New Zealand megafauna were not in decline before human colonization. Proc Natl Acad Sci U S A. 111:4922–4927.

Allentoft ME, Rawlence NJ. 2012. Moa's ark or volant ghosts of Gondwana? Insights from nineteen years of ancient DNA research on the extinct moa (Aves: Dinornithiformes) of New Zealand. Ann Anat. 194:36–51.

Allentoft, ME, et al. 2011. Profiling the dead: generating microsatellite data from fossil bones of

extinct megafauna–protocols, problems, and prospects. PLoS One 6:e16670.

Allentoft ME, et al. 2009. Identification of microsatellites from an extinct moa species using high-throughput (454) sequence data. BioTechniques 46:195–200.

Baker AJ, Haddrath O, McPherson JD, Cloutier A. 2014. Genomic support for a moa-tinamou clade and adaptive morphological convergence in flightless ratites. Mol Biol Evol. 31:1686–1696.

Baker AJ, Huynen LJ, Haddrath O, Millar CD, Lambert DM. 2005. Reconstructing the tempo and mode of evolution in an extinct clade of birds with ancient DNA: the giant moas of New Zealand. Proc Natl Acad Sci U S A. 102:8257–8262.

Bolger AM, Lohse M, Usadel B. 2014. Trimmomatic: a flexible trimmer for Illumina sequence data. Bioinformatics 30:2114–2120.

Bunce M, et al. 2009. The evolutionary history of the extinct ratite moa and New Zealand Neogene paleogeography. Proc Natl Acad Sci U S A. 106:20646–20651.

Bunce M, et al. 2003. Extreme reversed sexual size dimorphism in the extinct New Zealand moa *Dinornis*. Nature 425:172–175.

Burga A, et al. 2017. A genetic signature of the evolution of loss of flight in the Galapagos cormorant. Science 356:eaal3345.

Choi Y, Sims GE, Murphy S, Miller JR, Chan AP. 2012. Predicting the functional effect of amino acid substitutions and indels. PLoS One 7:e46688.

Cloutier A, et al. 2018. Phylogenomic analyses resolve historically contentious relationships within the Palaeognathae in the presence of an empirical anomaly zone. bioRxiv [DOI pending].

Cooper A, et al. 2001. Complete mitochondrial genome sequences of two extinct moas clarify

ratite evolution. Nature 409:704–707.

Cooper A, Poinar HN. 2000. Ancient DNA: do it right or not at all. Science 289:1139.

Cooper A, et al. 1992. Independent origins of New Zealand moas and kiwis. Proc Natl Acad Sci U S A. 89:8741–8744.

Dabney J, Meyer M, Pääbo S. 2013. Ancient DNA damage. Cold Spring Harb Perspect Biol. 5:a012567.

Faircloth BC. 2008. MSATCOMMANDER: detection of microsatellite repeat arrays and automated, locus-specific primer design. Mol Ecol Resour. 8:92–94.

Grealy A, Rawlence NJ, Bunce M. 2017. Time to spread your wings: a review of the avian ancient DNA field. Genes 8:184.

Haddrath O, Baker AJ. 2012. Multiple nuclear genes and retroposons support vicariance and dispersal of the palaeognaths, and an Early Cretaceous origin of modern birds. Proc Roy Soc B Biol Sci. 279:4617–4625.

Haddrath O, Baker AJ. 2001. Complete mitochondrial DNA genome sequences of extinct birds: ratite phylogenetics and the vicariance biogeography hypothesis. Proc Roy Soc B Biol Sci. 268:939–945.

Hagelberg E. 1994. Mitochondrial DNA from ancient bones. In: Hermann B, Hummell S, editors. *Ancient DNA: recovery and genetic analysis of genetic material from paleontological, archaeological, museum, medical, and forensic specimens.* New York: Springer-Verlag. p. 195–204.

Hahn C, Bachmann L, Chevreux B. 2013. Reconstructing mitochondrial genomes directly from genomic next-generation sequencing reads – a baiting and iterative mapping approach. Nucleic Acids Res. 41:e129.

Highnam G, Franck C, Martin A, Stephens C, Puthige A, Mittelman D. 2013. Accurate human microsatellite genotypes from high-throughput resequencing data using informed error profiles. Nucleic Acids Res. 41:e32.

Hillier LW, et al. 2004. Sequence and comparative analysis of the chicken genome provide unique perspectives on vertebrate evolution. Nature 432:695–716.

Hofreiter M, et al. 2015. The future of ancient DNA: technical advances and conceptual shifts. Bioessays 37:284–293.

Holdaway RN, et al. 2014. An extremely low-density human population exterminated New Zealand moa. Nat Commun. 5:5436.

Huson DH, et al. 2016. MEGAN Community Edition – interactive exploration and analysis of large-scale microbiome sequencing data. PLoS Comput Biol. 12:e1004957.

Huynen L, et al. 2014. Reconstruction and in vivo analysis of the extinct *tbx5* gene from ancient wingless moa (Aves: Dinornithiformes). BMC Evol Biol. 14:75.

Huynen L, Gill BJ, Millar CD, Lambert DM. 2010. Ancient DNA reveals extreme egg morphology and nesting behavior in New Zealand's extinct moa. Proc Natl Acad Sci U S A. 107:16201–16206.

Huynen L, Millar CD, Scofield RP, Lambert DM. 2003. Nuclear DNA sequences detect species limits in ancient moa. Nature 425:175–178.

Jónsson H, Ginolhac A, Schubert M, Johnson PLF, Orlando L. 2013. mapDamage2.0: fast approximate Bayesian estimates of ancient DNA damage parameters. Bioinformatics 29:1682–1684.

Katoh K, Standley DM. 2013. MAFFT multiple sequence alignment software version 7: improvements in performance and usability. Mol Biol Evol. 30:772–780.

Knapp M, Clarke AC, Horsburgh KA, Matisoo-Smith EA. 2012. Setting the stage – building and working in an ancient DNA laboratory. Ann Anat. 194:3–6.

Kojima K, Kawai Y, Misawa K, Mimori T, Nagasaki M. 2016. STR-realigner: a realignment method for short tandem repeat regions. BMC Genomics 17:991.

Kosakovsky Pond SL, Frost SDW, Muse SV. 2005. HyPhy: hypothesis testing using phylogenies. Bioinformatics 21:67–-679.

Langmead B, Salzberg SL. 2012. Fast gapped-read alignment with Bowtie 2. Nat. Methods 9:357–359.

Le Duc D, et al. 2015. Kiwi genome provides insights into evolution of a nocturnal lifestyle. Genome Biol. 16:147.

Li H, et al. 2009. The sequence alignment/map format and SAMtools. Bioinformatics 25:2078–2079.

Lunter G, Goodson M. 2011. Stampy: a statistical algorithm for sensitive and fast mapping of Illumina sequence reads. Genome Res. 21:936–939.

McCallum J, et al. 2013. Highly informative ancient DNA `snippets' for New Zealand moa. PLoS One 8:e50732.

Petit F, Sears KE, Ahituv N. 2017. Limb development: a paradigm of gene regulation. Nat Rev Genet. 18:245–258.

Phillips MJ, Gibb GC, Crimp EA, Penny D. 2010. Tinamous and moa flock together: mitochondrial genome sequence analysis reveals independent losses of flight among ratites. Syst Biol. 59:90–107.

Rawlence NJ, Wood JR, Armstrong KN, Cooper A. 2009. DNA content and distribution in ancient feathers and potential to reconstruct the plumage of extinct avian taxa. Proc Roy

Soc B Biol Sci. 276:3395–3402.

Sackton T, et al. 2018. Convergent regulatory evolution and the origin of flightlessness in palaeognathous birds. bioRxiv doi: https://doi.org/10.1101/262584.

Sawyer S, Krause J, Guschanski K, Savolainen V, Pääbo S. 2012. Temporal patterns of nucleotide misincorporations and DNA fragmentation in ancient DNA. PLoS One 7:e34131.

Selkoe KA, Toonen RJ. 2006. Microsatellites for ecologists: a practical guide to using and evaluating microsatellite markers. Ecol Lett. 9:615–629.

Simão FA, Waterhouse RM, Ioannidis P, Kriventseva EV, Zdobnov EM. 2015. BUSCO: assessing genome assembly and annotation completeness with single-copy orthologs. Bioinformatics 31:3210–3212.

Smith MD, et al. 2015. Less is more: an adaptive branch-site random effects model for efficient detection of episodic diversifying selection. Mol Biol Evol. 32:1342–1353.

Storey J. 2015. qvalue: Q-value estimation for false discovery rate control. R package version 2.0.0. http://qvalue.princeton.edu, http://github.com/jdstorey/qvalue.

Tanaka M. 2013. Molecular and evolutionary basis of limb field specification and limb initiation. Dev Growth Differ. 55:149–163.

Tickle C. 2015. How the embryo makes a limb: determination, polarity and identity. J Anat. 227:418–430.

Wertheim JO, Murrell B, Smith MD, Kosakovsky Pond SL, Scheffler K. 2015. RELAX: detecting relaxed selection in a phylogenetic framework. Mol Biol Evol. 32:820–832.

Wood JR, et al. 2013a. A megafauna's microfauna: gastrointestinal parasites of New Zealand's extinct moa (Aves: Dinornithiformes). PLoS One 8:e57315.

Wood JR, et al. 2013b. Resolving lost herbivore community structure using coprolites of four sympatric moa species (Aves: Dinornithiformes). Proc Natl Acad Sci U S A. 110:16910–16915.

Worthy TH, Holdaway RN. 2002. *The lost world of the moa: prehistoric life of New Zealand.* Bloomington: Indiana University Press.

Yang Z. 2007. PAML 4: phylogenetic analysis by maximum likelihood. Mol Biol Evol. 24:1586–1591.

Zakany J, Duboule D. 2007. The role of Hox genes during vertebrate limb development. Curr Opin Genet Dev. 17:359–366.

Zhang G, et al. 2014. Comparative genomic data of the avian phylogenomics project. GigaScience 3:26.

Table 1 Read mapping information for little bush moa sequencing libraries

	TruSeq libraries		Nextera libraries		
	CTTGTA	**GCCAAT**	**AGGCAG**	**CAGAGA**	**CTCTCT**
Raw reads (paired)	530,099,258	59,208,990	46,836,756	35,552,367	38,311,748
Trimmed reads					
Paired	486,360,442	57,743,619	45,142,645	34,079,453	36,434,453
Single	27,247,969	1,059,500	44,515	35,261	46,412
Alignment rate (MAPQ ≥ 30, %)	12.9	9.4	0.3	0.4	0.3
Duplicates (% of mapped)	69.4	98.7	75.0	81.9	73.7
Mean mapped read length (bp)[1]					
Paired	98.7	94.2	72.7	69.5	67.8
Single	84.2	69.7	86.7	63.0	49.6
Mean insert size (bp)[1]	206.8	274.0	90.4	78.6	74.9

[1]for de-duplicated reads

Table 2 Assembly statistics for emu reference and little bush moa nuclear genomes

	Emu	**Little bush moa**
No. Scaffolds	2,882	1,942
Total scaffold length (bp, gapped)	1,192,339,227	1,190,767,405
Total ACGT bases (bp)	1,179,147,775	889,712,222
No. Contigs	18,794	1,335,004
Contig N50 (bp)	189,906	1,126
Mean contig size (bp)	62,817	673
Avg. break between contigs (bp)	738	218
Total BUSCOs	4799/4915 (97.6%)	4289/4915 (87.3%)
Complete BUSCOs	4628/4915 (94.2%)	3693/4915 (75.1%)

Table 3 Tests of selection for candidate limb development genes

Gene	Description	CDS length (AA, % of total)			RELAX tests			
					Moa		All flightless	
		Chicken	Emu	Moa	K	P_{adj}	K	P_{adj}
a) Candidate limb development genes								
FGF8	Fibroblast growth factor 8	214	214	189 (88%)	3.912	0.991	49.994	0.081
FGF10	Fibroblast growth factor 10	212	212	204 (96%)	0.494	0.419	1.052	0.542
GLI3	GLI family zinc finger 3	1576	1575	1570 (99%)	1.491	0.389	0.359	0.006
HOXA1	Homeobox A1	320	319	308 (96%)	0.999	0.991	0.931	0.459
HOXA2	Homeobox A2	375	374	357 (95%)	0.178	0.074	3.424	< 0.001
HOXA3	Homeobox A3	413	413	414 (100%)	1.491	0.389	1.033	0.525
HOXA4	Homeobox A4	309	145†	155 (50%)	0.365	0.389	2.564	0.006
HOXA5	Homeobox A5	270	270	251 (93%)	29.348	0.289	0.633	0.215
HOXA6	Homeobox A6	231	231	231 (100%)	0.828	0.808	0.272	0.365
HOXA7	Homeobox A7	219	219	219 (100%)	28.556	0.389	1.156	0.425
HOXA9	Homeobox A9	260	261	249 (95%)	1.985	0.389	2.040	0.084
HOXA10	Homeobox A10	364	317†	289 (79%)	1.239	0.934	2.914	0.062
HOXA11	Homeobox A11	297	297	255 (86%)	0.303	0.389	1.453	0.110
HOXA13	Homeobox A13	290	290	269 (93%)	1.179	0.934	0.858	0.459
HOXD3	Homeobox D3	413	248†	247 (60%)	1.211	0.808	1.326	0.425
HOXD4	Homeobox D4	237	237	202 (85%)	1.125	0.966	9.667	0.006
HOXD8	Homeobox D8	268	147†	146 (54%)	0.607	0.497	< 0.001	0.379
HOXD9	Homeobox D9	302	299	283 (94%)	0.295	0.339	0.816	0.217
HOXD10	Homeobox D10	339	339	339 (100%)	0.923	0.991	49.998	0.152
HOXD11	Homeobox D11	280	282	272 (96%)	0.967	0.976	0.642	0.081
HOXD12	Homeobox D12	266	266	266 (100%)	1.452	0.397	1.006	0.569
HOXD13	Homeobox D13	301	82†	74 (25%)	0.926	0.991	0.939	0.525
SALL4	Spalt-like transcription factor 4	1108	1111	1023 (92%)	0.793	0.389	0.860	0.146
SHH	Sonic hedgehog	425	422	398 (94%)	1.979	0.389	0.974	0.542
TBX5	T-box 5	521	538	426 (79%)	0.240	0.389	1.021	0.545
WNT2B	Wnt family member 2B	385	330†	260 (68%)	0.636	0.339	1.703	0.081
b) Candidate genes from the Galapagos cormorant								
DCHS1	Dachsous cadherin-related 1	3266	3267	3090 (95%)	1.094	0.389	1.006	0.554
DVL1	Dishevelled segment polarity protein 1	712	655†	633 (89%)	1.326	0.397	0.814	0.127
DYNC2H1	Dynein cytoplasmic 2 heavy chain 1	4301	4295	3991 (93%)	1.152	0.389	0.763	0.089
EVC	EvC ciliary complex subunit 1	984	927†	871 (89%)	0.169	0.389	0.654	0.023
FAT1	FAT atypical cadherin 1	4645	4644	4489 (97%)	1.493	0.013	0.880	0.024
GLI2	GLI family zinc finger 2	1528	1528	1528 (100%)	0.408	0.013	0.927	0.262
IFT122	Intraflagellar transport 122	1245	1239	1202 (97%)	0.035	0.808	1.311	0.146
KIF7	Kinesin family member 7	1412	1279†	1226 (87%)	0.683	0.389	1.204	0.146
OFD1	OFD1, centriole and centriolar satellite protein	1012	1014	1002 (99%)	0.978	0.991	0.006	0.102
TALPID3	KIAA0586	1523	1527	1474 (97%)	0.748	0.389	0.035	0.023
WDR34	WD repeat domain 34	500	502	459 (91%)	18.909	0.251	0.776	0.102

K: Relaxation parameter (values < 1 indicate relaxed selection on foreground branches, values > 1 denote intensified selection)
P_{adj}: Adjusted P-value (Q-value) controlling for the false discovery rate at a significance level of 0.05 based on N= 37 genes tested
†Partial CDS recovered in the emu reference sequence

FIGURE CAPTIONS

Fig. 1 Endogenous DNA content across library preparations. A) Proportion of final nuclear genome assembly attributable to sequencing reads from each library. B) MEGAN assignment of taxonomic affiliations for individual sequencing reads. C) Proportions of reads assigned to avian species by taxonomic profiling compared to proportions mapped to the emu reference genome.

Fig. 2 Little bush moa genome assemblies. A) *De novo* assembled mitochondrial genome, with locations of annotated genes and RNAs indicated. Inward-facing plot shows per-base depth of coverage (DoC). B) Reference-based nuclear genome assembly. Alternating gray and blue sections along outer circle indicate individual scaffolds in order of decreasing size. Inward-facing plot shows depth of coverage calculated in ten non-overlapping windows per scaffold.

Fig. 3 Polymorphic microsatellite repeat identified from the little bush moa nuclear genome. A) Partial sequence for microsatellite anoDid_tri6 showing the consensus genome sequence in black, with mapped reads below. Partners belonging to the same read pair are shaded with the same color, while unpaired reads or those whose partner falls outside the illustrated region are shaded in gray. The microsatellite repeat region is boxed, showing the heterozygous GTT_7/GTT_9 genotype for this individual. B) Multiple sequence alignment with the corresponding genomic region from other ratites. The microsatellite repeat region is boxed.

Suppl. Fig. S1 Patterns of DNA damage estimated for reads mapping to the little bush moa nuclear (A, B) and mitochondrial (C, D) genomes are consistent with expectations for aDNA. A,C) Excess of purines immediately preceding strand breaks (note that observed coordinates for purine enrichment are shifted slightly relative to expectations likely due to some fragments resulting from DNA shearing during library preparation). B,C) Increased C-to-T transitions towards fragment edge.

Suppl. Fig. S2 Mitochondrial control region sequence corroborates taxonomic identity of the little bush moa specimen. Sequence from the current study is shown at the top, with reference little bush moa sequences aligned below. GenBank accessions for reference sequences are followed by specimen identifiers from Bunce et al. (2009), and dots indicate identity with the first alignment sequence. Samples originating from the South Island of New Zealand are shaded in blue, those from the North Island in yellow, and the control region 'snippet' of McCallum et al. (2013) is boxed.

Suppl. Fig. S3 The 4 amino acid deletion in *CUX1* of the Galapagos cormorant (*P. harrisi*) described by Burga et al. (2017) is not shared with other flightless birds (penguins and ratites).

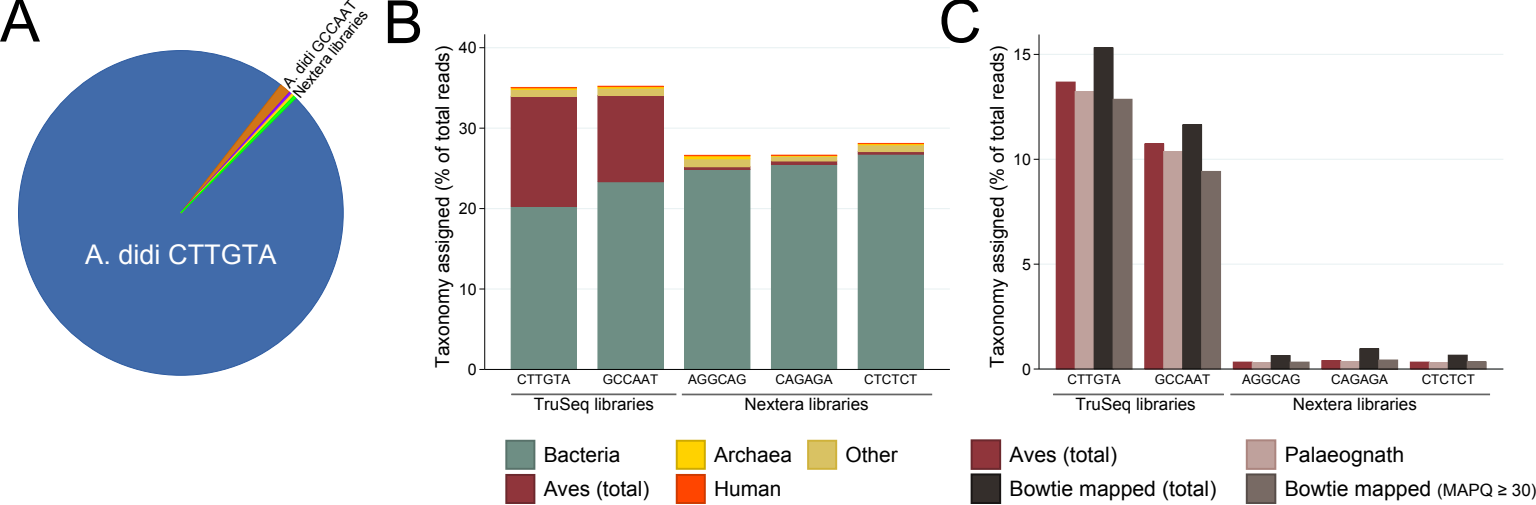
A
A. didi CTTGTA
A. didi GCCAAT
Nextera libraries
B
Taxonomy assigned (% of total reads)
0
10
20
30
40
CTTGTA
GCCAAT
AGGCAG
CAGAGA
CTCTCT
TruSeq libraries
Nextera libraries
C
Taxonomy assigned (% of total reads)
0
5
10
15
CTTGTA
GCCAAT
AGGCAG
CAGAGA
CTCTCT
TruSeq libraries
Nextera libraries
Bacteria
Archaea
Other
Aves (total)
Palaeognath
Aves (total)
Human
Bowtie mapped (total)
Bowtie mapped (MAPQ ≥ 30)

Fig. 1

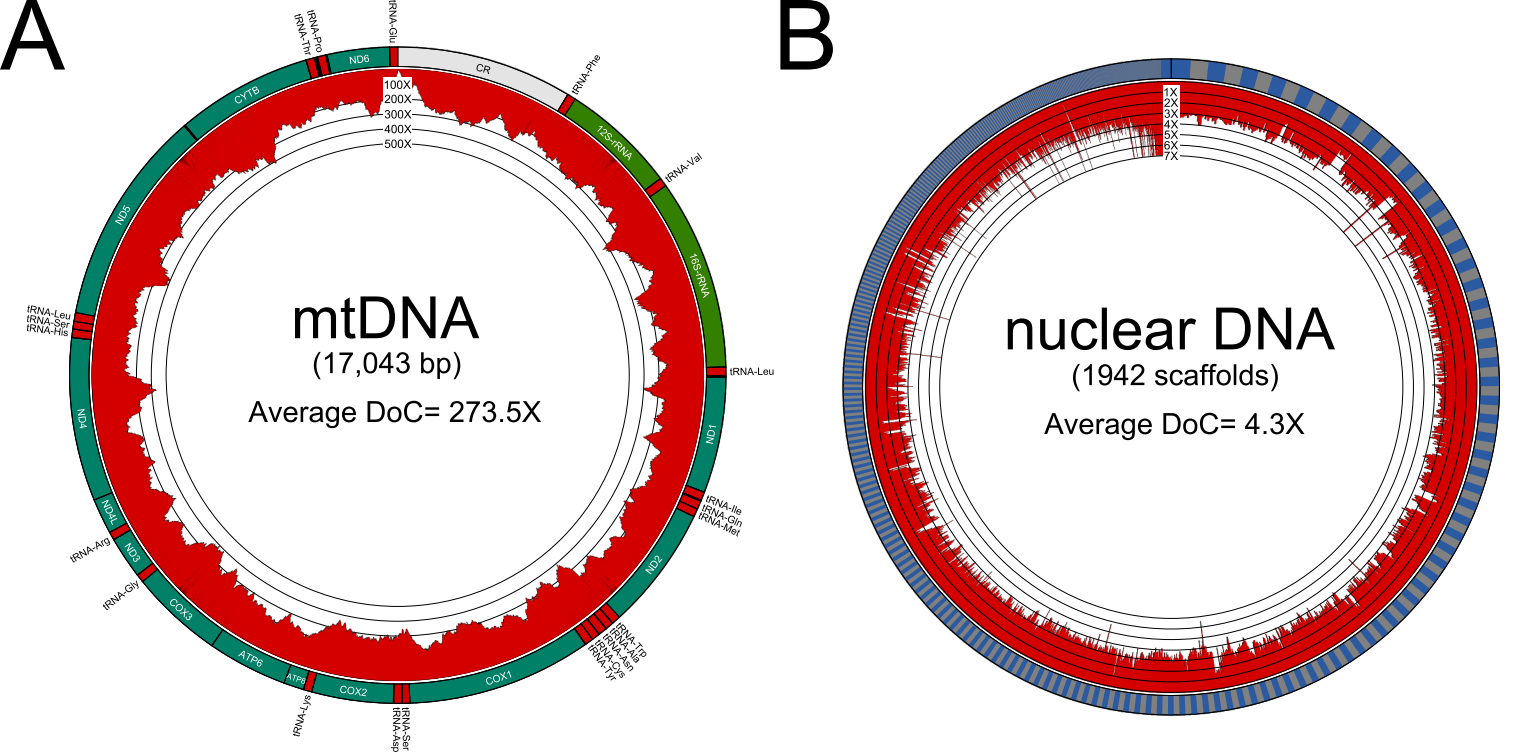
A
mtDNA
(17,043 bp)
Average DoC= 273.5X
100X
200X
300X
400X
500X
CR
tRNA-Phe
12S-RNA
tRNA-Val
16S-RNA
tRNA-Leu
ND1
tRNA-Ile
tRNA-Gln
tRNA-Met
ND2
tRNA-Trp
tRNA-Ala
tRNA-Asn
tRNA-Cys
tRNA-Tyr
COX1
tRNA-Ser
tRNA-Asp
COX2
tRNA-Lys
ATP8
ATP6
COX3
tRNA-Gly
ND3
tRNA-Arg
ND4L
ND4
tRNA-Leu
tRNA-Ser
tRNA-His
ND5
CYTB
ND6
tRNA-Pro
tRNA-Thr
tRNA-Glu
B
nuclear DNA
(1942 scaffolds)
Average DoC= 4.3X
1X
2X
3X
4X
5X
6X
7X

Fig. 2

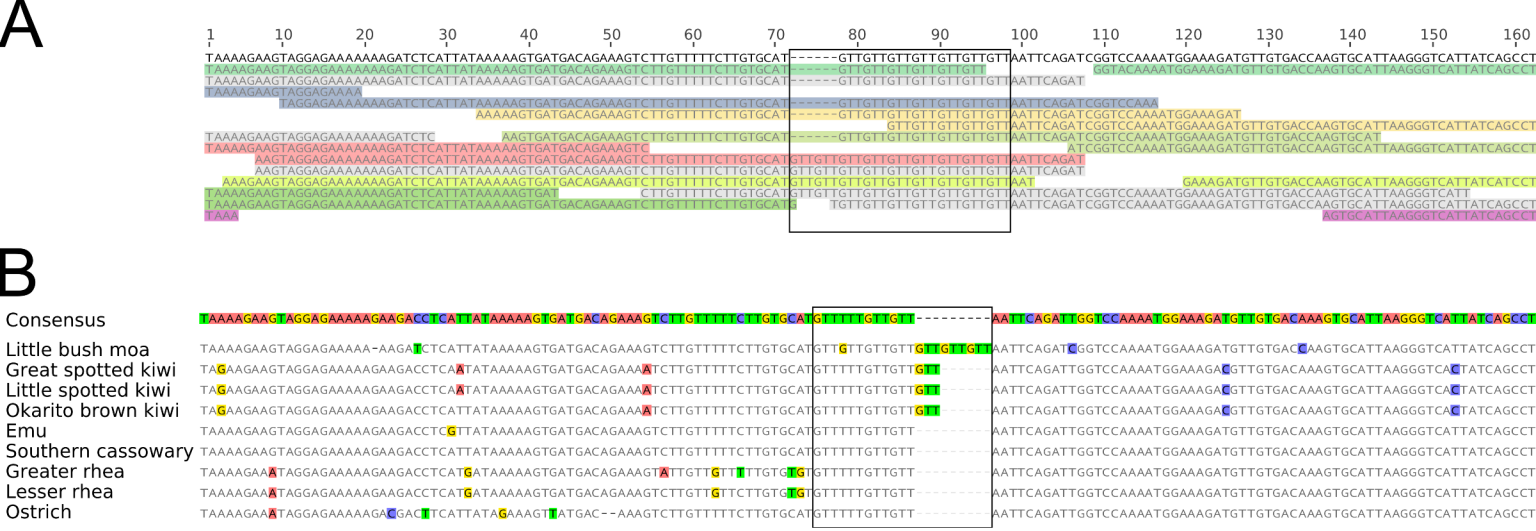
A
B
Consensus
Little bush moa
Great spotted kiwi
Little spotted kiwi
Okarito brown kiwi
Emu
Southern cassowary
Greater rhea
Lesser rhea
Ostrich

Fig. 3